Available online at http://www.ssstj.sci.ssru.ac.th

Suan Sunandha Science and Technology Journal

Utilization of Zinc-doped Nickel Oxide Hole Transporting Materials to Improve Efficiency and Stability of Perovskite Solar Cells

Piyapond Makming[1], Saowalak Homnan[2], Pipat Ruankham[2], Duangmanee Wongratanaphisan[2], Yothin Chimupala[3], Fabrice Goubard[4], Antoine Adjaoud[4], Akarin Intaniwet[1,*]

[1]School of Renewable Energy, Maejo University, San Sai District, Chiang Mai 50290, Thailand
[2]Department of Physics and Materials Science, Faculty of Science, Chiang Mai University, Chiang Mai 50200, Thailand
[3]Department of Industrial Chemistry, Faculty of Science, Chiang Mai University, Chiang Mai 50200, Thailand
[4]Laboratory of Physicochemistry of Polymers and Interfaces, CY Cergy Paris University, Cergy-Pontoise Cedex 95000, France

*Corresponding author e-mail: a.intaniwet@hotmail.co.th

Received: *1 March 2022* / **Revised**: *17 March 2022* / **Accepted**: *14 June 2022*

Abstract

Currently, several techniques have been employed in order to obtain a better quality of perovskite solar cells (PSCs). In this research, we focus on the development of the hole transporting material (HTM) for the efficiency as well as the stability enhancement of the PSCs. Here, a hole transporting layer (HTL) was fabricated using zinc-doped nickel oxide (Zn-doped NiO_x) nanoparticles and the HTL was incorporated into the cesium-formamidinium (CsFA) based PSCs to improve the electrical properties. As a result, PSCs with 1% Zn-doped NiO_x demonstrated the highest power conversion efficiency (PCE) up to 14.72% with an open-circuit voltage (V_{OC}), a short-circuit current density (J_{SC}) and a fill factor of 1.02 V, 19.59 mA/cm^2 and 0.734, respectively. Moreover, the PSCs with Zn-doped NiO_x showed an enhancement in shelf-stability under aging conditions. The physical properties of the Zn-doped NiO_x were analyzed using X-ray photoelectron spectroscopy (XPS) and transmission electron microscopy (TEM). The morphological characteristics of the HTL surface were examined by scanning electron microscopy (SEM) and the photovoltaic properties were analyzed in more detail.

Keywords: Perovskite solar cells, Doping, NiO_x, Zn, Hole transporting layers

1. Introduction

Perovskite solar cells (PSCs) have attracted tremendous attention in the field of energy as an emerging photovoltaic device with a high potential to rival the Si-based solar cells since the power conversion efficiency (PCE) of the PSCs has been sharply increased from 3.8%-25.2% over a short period of time and the device also offers low fabrication cost (Sahoo, Manoharan, & Sivakumar, 2018; Shahiduzzaman et al., 2020; Zhou, Zhou, Tian, Zhu, & Tu, 2018). High PCE can be attributed to the unique optoelectrical properties of the perovskite such as high light absorption ability, low exciton binding energy (Miyata et al., 2015), long carrier diffusion length and lifetime, and power generation stability (Meng, You, & Yang, 2018; Song, Yin, Li, & Li, 2021).

A regular PSC has a device structure of anode/electron transporting layer (ETL)/perovskite/hole transporting layer (HTL)/cathode (Sahoo et al., 2018). The state-of-the-art PSCs mostly require organic HTL such as spiro-OMeTAD (Jeon et al., 2018). Although the air stability of spiro-OMeTAD-based PSCs has been extended up to several hours, the cost of spiro-OMeTAD (500 USD/gm) is extremely high and also the thermal stability and preparation methods remain unsolvable (Serhan et al., 2019). Alternatively, inorganic HTMs such as

Suan Sunandha Science and Technology Journal

CuI, pristine- or doped-NiO_x, Cu_2O, CuSCN, $CsSnI_3$, etc., have been employed as the HTL for PSCs (Kim et al., 2020; Yang & Park, 2019; Yin et al., 2016) owing to their low-cost. Interestingly, inorganic HTL materials offer advantages in terms of light and thermal stability, especially moisture stability. Though, crucial contributions are still needed to achieve long-term stability.

This study focuses on the application of zinc-doped nickel oxide (Zn-doped NiO_x) nanoparticles as the HTL to improve the efficiency and the stability of PSCs. Zn-doped NiO_x film was deposited from a colloidal solution of Zn-doped NiO_x nanoparticles in the non-polar isopropanol (IPA) solvent, which will not interact with the perovskite layer. The physical properties of the Zn-doped NiO_x were analyzed using X-ray photoelectron spectroscopy (XPS) and transmission electron microscopy (TEM). The crystal structure was determined using X-ray diffraction (XRD). The morphological characteristics of the HTL surface were examined by scanning electron microscopy (SEM). Finally, the devices were tested under the solar simulator to measure the current density-voltage (J-V) characteristics and the efficiency of the device was determined.

2. Experimental

2.1 NiO_x and NiO_x doped Zn nanoparticles preparation

Zn-doped NiO_x nanoparticles were prepared by a solvothermal method. In the beginning, 0.65 g of nickel acetylacetonate ($Ni(acac)_2$) and $Zn(C_5H_7O_2)_2{\cdot}H_2O$ (1.0 mol%) was added to 70 ml of *tert*-butanal in a conical flask [11]. The mixture was put on a hotplate and stirred at 70°C for 10 h. The resulting turbid green solution was transferred into a Teflon-lined stainless-steel autoclave with 100 ml capacity. Then the sample was kept in an oven at 210°C for 24 h. After cooling to room temperature, the resulting NiO_x colloidal solution was centrifuged. The precipitate was washed with absolute ethanol two times. Then, the NiO_x nanoparticles were dried at 75°C for 2 h in an oven. Finally, the NiO_x nanoparticles were sintered at 300°C for 2 h. It is noted that all processes were conducted in ambient air conditions.

2.2. Fabrication of perovskite solar cells

FTO-coated glass substrates were cleaned sequentially with Alconox, de-ionized (DI) water, acetone, and isopropanol using the ultrasonic sonicator for 30 min. Then, the FTO substrates were treated with UV-ozone for 15 min. An electron-transporting zinc-tin oxide (ZTO) layer was deposited by spin-coating a 0.3M solution of zinc acetate dihydrate and tin (II) 2-ethylhexanoate with equivalent molar of ethanolamine in 2-methoxyethanol onto the cleaned FTO-coated glass at 3000 rpm for 30 s. The as-deposited film was then annealed on a hotplate in the ambient atmosphere for 1 h at 450°C (Zhao et al., 2012). Next, the substrates were cooled to room temperature, and the ZTO films were treated with UV-O_3 to clean the surface.

A $Cs_{0.17}FA_{0.83}Pb(I_{0.83}Br_{0.17})_3$ or CsFA perovskite solution was prepared with the procedure reported in the literature (Schutt et al., 2019). The CsFA film was deposited via a two-step spin-coating process at 1000 rpm and 6000 rpm for 10 s and 20 s, respectively. During the second step, 120 µL of anisole was dripped on the spinning substrate 10 s before the end of the procedure. The samples were then annealed on a hotplate at 100°C for 15 min and were thermalized to room temperature. Subsequently, 60 µL of Zn-doped NiO_X nanoparticles solution (5 mg mL^{-1} in absolute isopropanol) was spin-coated at 3000 rpm for 30 s onto the CsFA perovskite layer and then 60 µL of CuSCN solution (35 mg mL^{-1} in diethyl sulfide) was coated at 2500 rpm for 30 s (Er, Icli, & Ozenbas, 2020; Zhao et al., 2012) to complete the HTL layer. Finally, the carbon electrode sheet was prepared by the ethanol solvent interacting process for 2 h, and then it was hot-pressed onto the CuSCN layer at 50°C for 3 min with pressure of 6 MPa (Passatorntaschakorn et al., 2021; Zhang et al., 2018) to finish the device. The other two PSCs were made to compare the result of different HTL compositions where only CuSCN and NiOx/CuSCN with similar coating conditions were used as the HTL.

2.3. Characterization

Elemental characterization was carried out for the NiO_x, NiO_x-Zn1% films using X-ray Photoelectron Spectroscopy (XPS) analysis and transmission electron microscopy (TEM) was used to observe the morphology. Moreover, the morphological characteristics of the HTL surface were examined by scanning electron microscopy

Suan Sunandha Science and Technology Journal

(SEM) on JEOL JSM-IT800. Current density-voltage (J-V) characteristics of PSCs were obtained from parameter analyzer (X200 source meter, Ossila) under AM 1.5 G (100 mW cm^{-2}) solar simulator. External quantum efficiency (EQE) spectra were measured using the QE-R quantum efficiency system (Enlitech) in a DC mode. The system was calibrated using a Si photodiode prior to the measurement. Electrochemical impedance spectra (EIS) were recorded using Auto lab PGSTAT 302 N and the equivalent circuit was used to fit the experimental data to extract the EIS parameters.

3. Results and Discussion

3.1 Physical properties

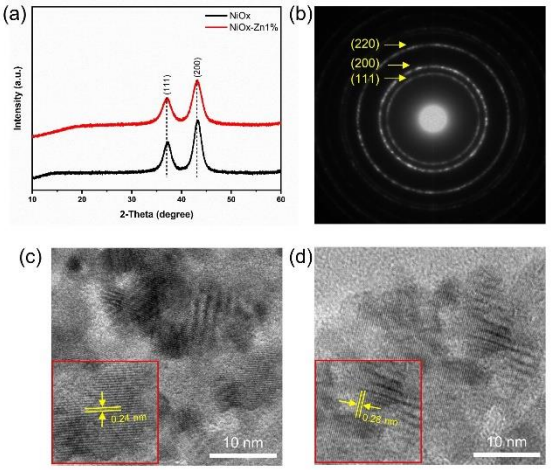

Figure 1. (a) XRD patterns of the as-synthesized NiO_x and NiO_x-Zn1%, (b) SAED pattern, TEM micrographs of (c) NiO_x and (d) NiO_x-Zn1% nanoparticles.

Figure 1a shows the XRD pattern of the as-synthesized NiO_x and NiO_x-Zn1% nanoparticles. It can be seen that two main NiO_x peaks at 37.24, and 43.4°, which refer to planes (1 1 1), and (2 2 0), and two main NiOx-Zn1% peaks at 37.01, and 43.19°, which refer to planes (1 1 1), and (2 2 0), are observed and the existence of the cubic bunsenite NiO_x phase is confirmed. Furthermore, X-ray diffraction results also indicate the presence of Zn in NiO_x since the peak of NiO_x-Zn1% is slightly shifted to the left. That means Zn can successfully be incorporated into the NiO_x nanoparticles without changing their structure (Mahmud Hasan et al., 2020; Xie et al., 2018). Selected-area electron diffraction (SAED) pattern and high-resolution TEM images of NiO_x and NiO_x-Zn1% are shown in Figure. 1b-d. The results demonstrate that NiO_x and NiO_x-Zn1% show a cubic crystalline structure with the distance between two successive bright fringes of 0.24 and 0.28 nm, respectively, which corresponds to the (111) plane of NiO_x (Nam et al., 2019).

Additionally, X-ray photoelectron spectroscopy (XPS) measurements were used to verify the doping result from the chemical composition of Zn-doped NiO_X films. Figure 2a shows the elemental composition and the survey XPS spectra of the films. It is noted that O and C elements are observed in every sample. The Zn element, on the other hand, is not detected in the film since only a small fraction of Zn (1%) was doped into the sample. Figure 2b exhibits the XPS spectrum of the Ni 2p peak in an undoped and doped Zn. The spectrum can be de-convoluted into six distinct peaks; 853.5, 854.8, 855.8, 871.1, 872.1, and 873.2 eV respectively (Chakrabarti et al., 2019), which indicate a normal state of Ni^{2+}. Figure. 2c shows the characteristic C 1s peak from the carbon film. All samples show four peak components centered at 284.4, 285.2, 286.7, and 288.6 eV, which correspond to the Ni–O, the interstitial Ni, C–C and C–H of acac ligand of residues of $Ni(acac)_2$ precursor, respectively. Furthermore, C–OH/C–O–C (286.7 eV) (Koshtyal et al., 2019) is slightly seen. Figure 2d shows the XPS spectrum for O 1s where four peaks can be de-convoluted from the spectrum centered at 529.0, 530.6, 532.6, and 531.8 eV respectively. The peak centered at 529.0 eV can be assigned to Ni-O octahedral bonding in NiO and the peak centered at 532.6 eV is likely due to the presence of nickel hydroxides or the surface adsorbed hydroxyl groups (Ratcliff et al., 2011).

Suan Sunandha Science and Technology Journal

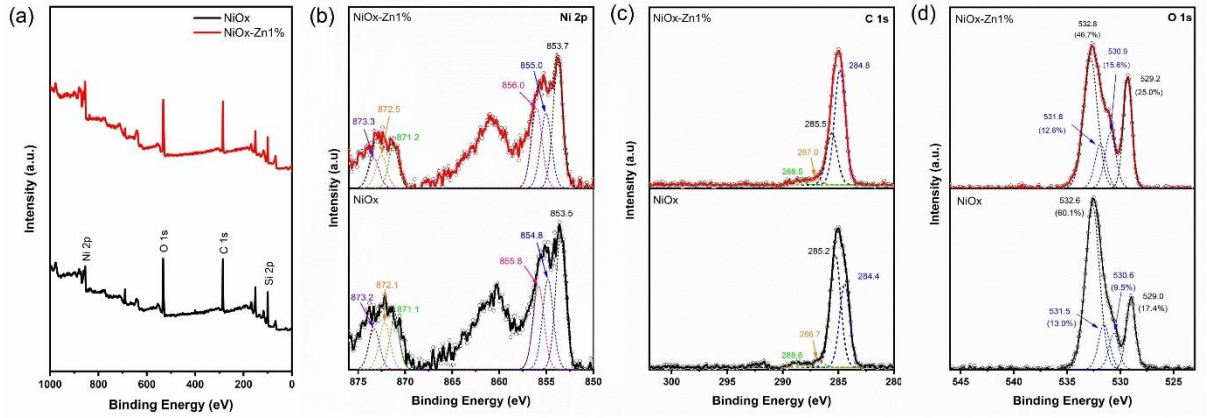

Figure 2. Compositional analysis of NiO_x and NiO_x-Zn1% nanoparticles. (a) Survey XPS spectra, and high-resolution XPS peaks of (b) Ni 2p, (c) C 1s, and (d) O 1s.

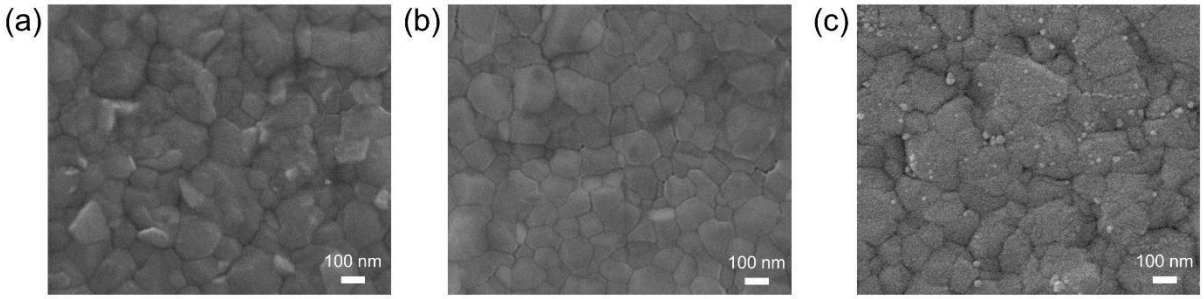

Figure 3. Top view SEM micrograph of (a) reference (CuSCN HTL) cell, (b) NiO_x/CuSCN HTL cell, and (c) NiO_x-Zn1%/CuSCN HTL cell.

Top view SEM surface morphology of different HTLs coated on perovskite layers presented in Figure 3a-c. The reference cell (Figure 3a), where only CuSCN was used for HTL, showed a rough and unsmooth surface with possible existence of pinholes. The NiO_x/CuSCN HTL (Figure 3b), on the other hand, provided a rather smooth surface layer with less grain boundary. Figure 3c shows the NiO_x-Zn1% film on a perovskite substrate. It can be seen that the surface layer was well covered, and the pinholes disappeared. The tiny white granule in the figure could be attributed to NiO_x-Zn1

Suan Sunandha Science and Technology Journal

3.2 Electrical properties

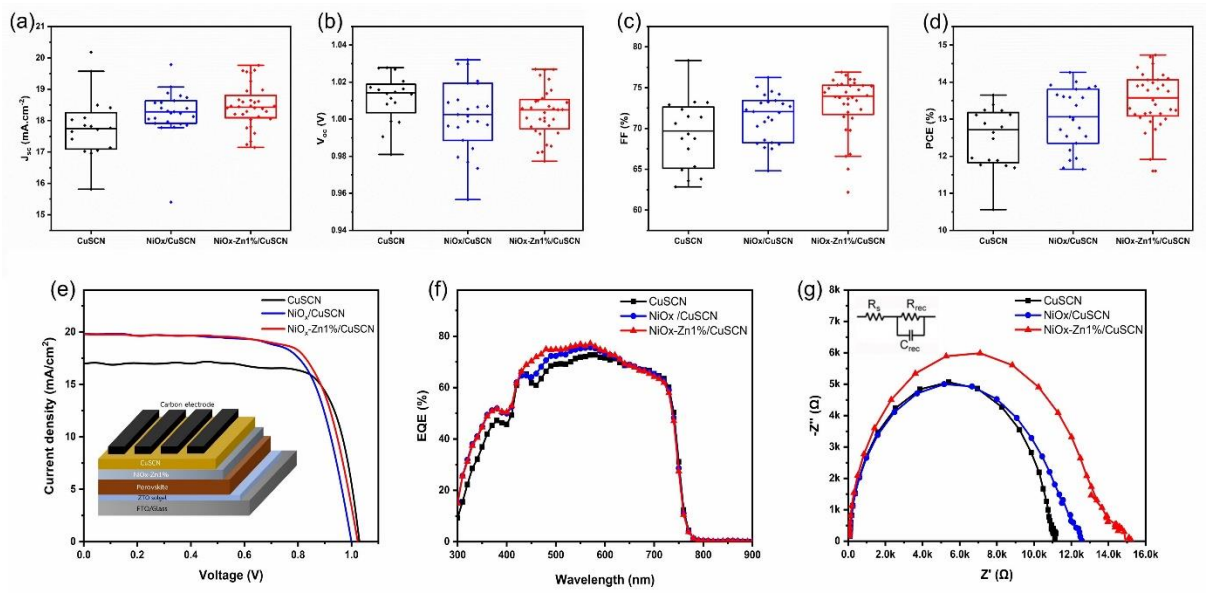

Figure 4. Box plots of photovoltaic parameters; (a) J_{SC}, (b) V_{OC}, (c) FF, and (d) PCE of PSCs fabricated based on conventional CuSCN, NiO_x/CuSCN and NiO_x-Zn1%/CuSCN HTLs; (e) J-V characteristics of the champion devices; (f) EQE curves of PSCs; (g) Nyquist plots under the forward bias of 0.85 V.

The photovoltaic parameters of the PSCs based on FTO/ZTO sol-gel/$Cs_{0.17}FA_{0.83}Pb(I_{0.83}Br_{0.17})_3$/$NiO_x$, NiO_x-Zn1%/CuSCN/carbon are displayed in Figure. 4(a-d) and in Table 1. The J-V curves of the champion PSCs are shown in Figure. 4e. The device with NiO_x-Zn1%/CuSCN film as HTL exhibited the best performance with the PCE values of 14.72%, short circuit current density (J_{sc}) of 19.59 mA /cm^2, open-circuit voltage (V_{oc}) of 1.02 V, and fill factor (FF) of 0.734 while the device with CuSCN, and NiO_x/CuSCN exhibited the maximum PCE values of 13.65%, and 14.26%, respectively. The PCE of the device with CuSCN as HTL was relatively low compared to other devices because there were still holes and uneven surface area, resulting in insufficient charge transport. However, with the addition of a Zn-doped NiO_x layer, the quality of the film seems to be improved and hence a higher conversion efficiency is acquired. Although, the maximum FF of 0.783, which was obtained from one time measurement from CuSCN device, is slightly higher than that of the champion NiO_x-Zn1%/CuSCN device (0.734) but the average photovoltaic parameters, as demonstrated in Table 1 in brackets, reveals that the device with Zn-doped NiO_x device offers the highest values. Figure 4f exhibits the EQE spectra obtained from devices. The EQE spectra show approximately 0.727, 0.757, and 0.771 respectively in the wavelength range of 500–800 nm. This results in a high J_{sc} which is in good agreement with the values obtained from the J–V measurement.

The electrochemical impedance spectroscopy (EIS) spectra was employed to further investigate the reason behind the photovoltaic parameter variation of the PSCs based on CuSCN, NiO_x/CuSCN, and NiO_x-Zn1%/CuSCN films. The Nyquist plots of the experimental data (Figure. 4g) were fitted using an equivalent circuit (inset of Figure. 4g) and EIS parameters, including series resistance (R_s), recombination resistance (R_{rec}), and chemical capacitance (C_{rec}). It was found that the R_{rec} of the PSCs based on NiO_x-Zn1%/CuSCN film (15.21 kΩ) was higher than both the PSCs based on CuSCN film (11.12 kΩ), and the PSCs based on NiO_x/CuSCN film (12.56 kΩ). Improving the interfacial region in the NiO_x-Zn1%/CuSCN device was probably the reason for the better photovoltaic parameters.

Suan Sunandha Science and Technology Journal

Table 1. Photovoltaic parameters of PSCs fabricated from CuSCN, NiO_x/CuSCN and NiO_x-Zn1%/CuSCN HTLs.

HTL	J_{sc} (mA/cm^2)	V_{oc} (V)	FF (%)	PCE (%)
CuSCN	16.95	1.027	78.33	13.65
	(17.82 ± 1.04)	(1.011 ± 0.013)	(69.31 ± 4.38)	(12.47 ± 0.84)
NiO_x/CuSCN	19.78	0.996	72.3	14.26
	(18.23 ± 0.78)	(1.001 ± 0.019)	(71.35 ± 2.96)	(13.03 ± 0.67)
NiO_x-Zn1%/CuSCN	19.59	1.023	73.42	14.72
	(18.46 ± 0.68)	(1.003 ± 0.013)	(72.96 ± 3.53)	(13.51 ± 0.74)

J_{sc}: short circuit current density, V_{oc}: open-circuit voltage, FF: fill factor, PCE: power conversion efficiency

The unencapsulated PSCs with the use of the CuSCN, NiO_x/CuSCN, and NiO_x-Zn1%/CuSCN HTL were tested in terms of shelf stability by measuring their photovoltaic properties of the devices stored in a desiccator with controlled environment (relative humidity of 40-50% and temperature of 25-30°C). As shown in Figure 5a and b, the PSC with the CuSCN HTL exhibits greater efficiency degradation when compared to the devices with NiO_x/CuSCN, and NiO_x-Zn1%/CuSCN HTLs. We note that there was a small increase of the PCE during the first few days of storing. We speculate that the surface stoichiometry of NiO_x might be modified by oxygen molecules in the air. This modification could facilitate the hole transport and extraction ability (Cao et al., 2017). In contrast, the efficiency of the PSCs with NiO_x/CuSCN or the NiO_x-Zn1%/CuSCN HTL decreased to less than 80% or 75% of its initial values after storing for 90 days (Figure. 5b). Although the slightly greater efficiency degradation was observed for the PSCs with NiO_x-Zn1%/CuSCN HTL when compared to the device without Zn doping. The actual average cell efficiency of NiO_x-Zn1%/CuSCN devices was comparable to that of the NiO_x/CuSCN devices. A reason behind this slightly larger efficiency degradation is still unclear. The investigation will be further performed. However, it can imply from the obtained results that the insertion of NiO_x or NiO_x-Zn1% nanoparticles between the perovskite layer and the CuSCN layer could significantly improve the shelf stability.

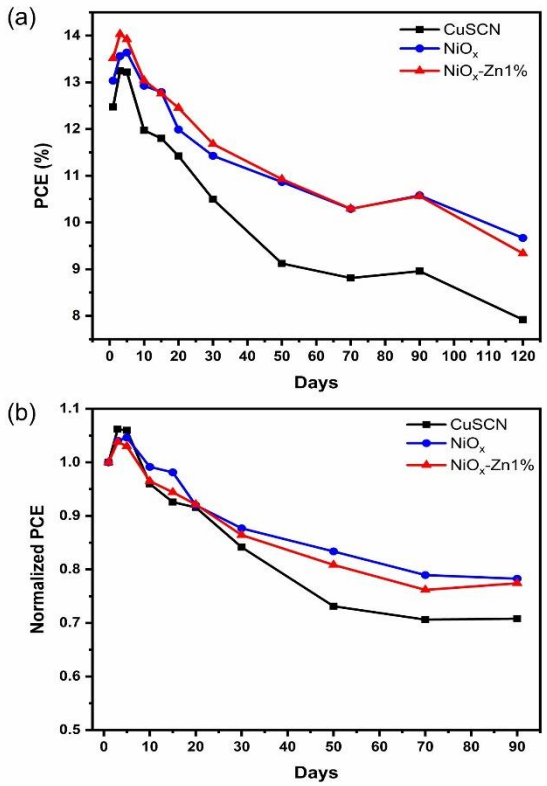

Figure 5. (a) Average PCE and (b) normalized PCE as a function of storage time for CuSCN-, NiO_x/CuSCN- and NiO_x-Zn1%/CuSCN-coated PSCs without encapsulation.

4. Conclusions

In conclusion, we have demonstrated that the Zn-doped NiO_x/CuSCN double inorganic material might be a promising material for holes extraction layer. PSC using Zn-doped NiO_x HTL reached a maximum PCE of 14.72%. The developed Zn-doped NiO_x non-polar interfacial layer could protect the perovskite layer during CuSCN deposition from the polar solvent. The air stability of the device under the ambient condition could be extended for more than 3 months with the efficiency

Suan Sunandha Science and Technology Journal

reduction of about 25%. The present study offers the alternative approach towards the development of highly air thermal stable, additive-free, low-cost based in real, cost-effective perovskite solar cells.

5. Acknowledgements

This work was financially supported by Maejo University and Chiang Mai University. The authors would like to thank the School of Renewable Energy, Maejo University, for the scholarship support and research grants for researchers.

6. References

Cao, J., Yu, H., Zhou, S., Qin, M., Lau, T. K., Lu, X., ... Wong, C. P. (2017). Low-temperature solution-processed NiO_X films for air-stable perovskite solar cells. *Journal of Materials Chemistry A*, *5*(22), 11071-11077. doi:10.1039/c7ta02228j

Chakrabarti, S., Carolan, D., Alessi, B., Maguire, P., Svrcek, V., & Mariotti, D. (2019). Microplasma-synthesized ultra-small NiO nanocrystals, a ubiquitous hole transport material. *Nanoscale Advances*, *1*, 4915-4925. doi:10.1039/c9na00299e

Er, U., Icli, K. C., & Ozenbas, M. (2020). Spin-coated copper(I) thiocyanate as a hole transport layer for perovskite solar cells. *Journal of Solid State Electrochemistry*, *24*, 293-304. doi:10.1007/s10008-019-04430-2

Jeon, N. J., Na, H., Jung, E. H., Yang, T. Y. Lee, Y. G., Kim, G., ... Seo, J. (2018). A fluorene-terminated hole-transporting material for highly efficient and stable perovskite solar cells. *Nature Energy*, *3*, 682-689. doi:10.1038/s41560-018-0200-6

Kim, J., Lee, Y., Gil, B., Yun, A. J., Kim, J., Woo, H., ... Park, B. (2020). A Cu_2O-CuSCN nanocomposite as a hole-transport material of perovskite solar cells for enhanced carrier transport and suppressed interfacial degradation. *ACS Applied Energy Materials*, *3*, 7572-7579. doi:10.1021/acsaem.0c01001

Koshtyal, Y., Nazarov, D., Ezhov, I., Mitrofanov, I., Kim, A., Rymyantsev, A., ... Maximov, M. (2019). Atomic layer deposition of NiO to produce active material for thin-film lithium-ion batteries. *Coatings*, *9*(5), 301. doi:10.3390/coatings9050301

Mahmud Hasan, A. K., Raifuku, I., Amin, N., Ishikawa, Y., Sarkar, D. K., Sobayel, K., ... Akhtaruzzaman, M. (2020). Air-stable perovskite photovoltaic cells with low temperature deposited NiOx as an efficient hole-transporting material. *Optical Materials Express*, *10*(8), 1801-1816. doi:10.1364/ome.391321

Meng, L., You, J., & Yang, Y. (2018). Addressing the stability issue of perovskite solar cells for commercial applications. *Nature Communications*, *9*, 5265. doi:10.1038/s41467-018-07255-1

Miyata, A., Mitioglu, A., Plochocka, P., Portugall, O., Wang, J. T. W., Stranks, S. D., ... Nicholas, R. J. (2015). Direct measurement of the exciton binding energy and effective masses for charge carriers in organic-inorganic tri-halide perovskites. *Nature Physics*, *11*, 582-587. doi:10.1038/nphys3357

Nam, V. B., Shin, J., Yoon, Y., Giang, T. T., Kwon, J., Suh, Y. D., ...Lee, D. (2019). Highly stable Ni-based flexible transparent conducting panels fabricated by laser digital patterning. *Advanced Functional Materials*, *29*(8), 1806895. doi:10.1002/adfm.201806895

Passatorntaschakorn, W., Bhoomanee, C., Ruankham, P., Gardchareon, A., Songsiriritthigul, P., & Wongratanaphisan, D. (2021). Room-temperature carbon electrodes with ethanol solvent interlacing process for efficient and stable planar hybrid perovskite solar cells. *Energy Reports*, *7*, 2493-2500. doi:10.1016/j.egyr.2021.04.031

Ratcliff, E. L., Meyer, J., Steirer, K. X., Garcia, A., Berry, J. J., Ginley, D. S., ... Armstrong, N. R. (2011). Evidence for near-surface NiOOH

Suan Sunandha Science and Technology Journal

species in solution-processed NiO_x selective interlayer materials: Impact on energetics and the performance of polymer bulk heterojunction photovoltaics. *Chemistry of Materials*, *23*, 4988-5000. doi:10.1021/cm202296p

Sahoo, S. K., Manoharan, B., & Sivakumar, N. (2018). Introduction: Why perovskite and perovskite solar cells? In S. Thomas, & A. Thankappan (Eds.), *Perovskite photovoltaics* (pp. 1-24). Academic Press. doi:10.1016/B978-0-12-812915-9.00001-0

Schutt, K., Nayak, P. K., Ramadan, A. J., Wenger, B., Lin, Y. H., & Snaith, H. J. (2019). Overcoming zinc oxide interface instability with a methylammonium-free perovskite for high-performance solar cells. *Advanced Functional Materials*, *29*(47), 1900466. doi:10.1002/adfm.201900466

Serhan, M., Sprowls, M., Jackemeyer, D., Long, M., Perez, I. D., Maret, W., ... Forzani, E. (2019). Total iron measurement in human serum with a smartphone. *AIChE Annual Meeting, Conference Proceedings*, *2019*. doi:10.1039/x0xx00000x

Shahiduzzaman, M., Fukaya, S., Muslih, E. Y., Wang, L., Nakano, M., Akhtaruzzaman, M., ... Taima, T. (2020). Metal oxide compact electron transport layer modification for efficient and stable perovskite solar cells. *Materials*, *13*(9), 2207. doi:10.3390/ma13092207

Song, J. X., Yin, X. X., Li, Z. F., & Li, Y. W. (2021). Low-temperature-processed metal oxide electron transport layers for efficient planar perovskite solar cells. *Rare Metals*, *40*, 2730-2746. doi:10.1007/s12598-020-01676-y

Xie, X., Gao, C., Du, X., Zhu, G., Xie, W., Liu, P., & Tang, Z. (2018). Improved optical and electrochromic properties of NiO_x films by low-temperature spin-coating method based on NiO_x nanoparticles. *Materials*, *11*(5), 760. doi:10.3390/ma11050760

Yang, G., & Park, S. J. (2019). Conventional and microwave hydrothermal synthesis and application of functional materials: A review. *Materials*, *12*(7), 1177. doi:10.3390/ma12071177

Yin, X., Liu, J., Ma, J., Zhang, C., Chen, P., Que, M., ... Shao, J. (2016). Solvothermal derived crystalline NiO_x nanoparticles for high performance perovskite solar cells. *Journal of Power Sources*, *329*, 398-405. doi:10.1016/j.jpowsour.2016.08.102

Zhang, H., Xiao, J., Shi, J., Su, H., Luo, Y., Li, D., ... Meng, Q. (2018). Self-adhesive macroporous carbon electrodes for efficient and stable perovskite solar cells. *Advanced Functional Materials*, *28*(39), 1802985. doi:10.1002/adfm.201802985

Zhao, Y., Dong, G., Duan, L., Qiao, J., Zhang, D., Wang, L., & Qiu, Y. (2012). Impacts of Sn precursors on solution-processed amorphous zinc-tin oxide films and their transistors. *RSC Advances*, *2*, 5307-5313. doi:10.1039/c2ra00764a

Zhou, D., Zhou, T., Tian, Y., Zhu, X., & Tu, Y. (2018). Perovskite-based solar cells: Materials, methods, and future perspectives. *Journal of Nanomaterials*, *2018*, 1-15. doi:10.1155/2018/8148072